Inorganic Chemistry

Article

pubs.acs.org/IC

# Crystalline and Glassy Phases in the Cs/Bi/As/S System

Tarun K. Bera,[†] Ratnasabapathy G. Iyer,[‡] Christos D. Malliakas,[†] and Mercouri G. Kanatzidis*[,†,§]

[†]Department of Chemistry, Northwestern University, Evanston, Illinois 60208, United States

[§]Materials Science Division, Argonne National Laboratory, Argonne, Illinois 60439, United States

[‡]Department of Chemistry, Claflin University, Orangeburg, South Carolina 29118, United States

Supporting Information

**ABSTRACT:** The quaternary $Cs_2S/Bi/As/S$ system was studied in an attempt to introduce two different asymmetric but isoelectronic building units, namely, $[Bi^{III}_xS_y]$ and $[As^{III}_xS_y]$, in a single structure. Reactions with a comparatively lower equivalent of arsenic in the $Cs_2S/Bi/As/S$ mixture led to the crystalline compound $Cs_3Bi(AsS_4)_2$. The structure features tetrahedral $[As^VS_4]^{3-}$ connected to $Bi^{III}$ centers to give infinite $^1/_\infty[Bi(AsS_4)_2^{3-}]$ chains. When the basicity was raised in these low arsenic fluxes by increasing the $Cs_2S$ fraction, the crystalline compound $Cs_9Bi(AsS_4)_4$, also featuring $[As^VS_4]^{3-}$ anions, was formed. On the other hand, arsenic-rich mixtures of $Cs_2S/Bi/As/S$ led to the formation of the glassy phase $Cs_2BiAs_3S_7$, which contains $As^{III}$ species. X-ray photoelectron spectroscopy (XPS), Raman spectroscopy, and pair distribution function (PDF) analysis indicate the presence of $As^{III}$-containing $[As_nS_{2n+1}]$ fragments in the glass structure. Several glasses in the series $Cs_{n-1}BiAs_nS_{2n+1}$ were also prepared using solid-state fusion reactions. The band gaps of the $Cs_{n-1}BiAs_nS_{2n+1}$ glasses are in the range of 1.51−1.81 eV, while that of the crystalline compound $Cs_3Bi(AsS_4)_2$ is ∼2.33 eV. The thermal and optical behaviors of these compounds are correlated with their structures and building units.


## INTRODUCTION

In recent years, we have established the utility of the molten polychalcogenide flux technique to synthesize a number of chalcoarsenate compounds featuring various $[As_xQ_y]^{n-}$ (Q = S, Se) anions containing arsenic in III and V oxidation states.[1] Particularly interesting is the pyramidal $[AsQ_3]^{3-}$ anion, with arsenic in the 3+ oxidation state, which when stabilized in a noncentrosymmetric structure has shown strong nonlinear-optical and second-harmonic-generation responses.[2] The interest in $[AsQ_3]^{3-}$-containing compounds also stems from the enhancement of glass-forming abilities provided by the more polarizable lone pair of electrons on arsenic and the strong covalency of the As−Q bonds.[3] Chalcogenide glasses containing As and Q have been the subject of extensive research because of their good infrared transparency, high refractive index, and long-term stability.[4] Furthermore, chalcogenide glasses are an important source of materials for IR detectors, lenses, and waveguides.[5] Our investigation was focused on understanding the flux chemistry[6a] and the controlling factors for stabilizing $As^{III}$ vis-à-vis $As^V$ in the resulting compounds. Previously, we have demonstrated that an arsenic-rich polychalcogenide flux favors the more reducing species $As^{III}$ instead of $As^V$ such as $AEuAsS_3$ (A = Li, K, Rb, Cs) and $Na_2EuAs_2S_5$, whereas an arsenic-poor flux favors the $As^V$ state in $NaEuAsS_4$ and $Na_4Eu(AsS_4)_2$.[6b,c] Further control in this chemistry is provided by the flux basicity determined by the alkali metal used; more basic metals favor higher oxidation states of arsenic.

The development of bismuth chalcoarsenate compounds is limited. Such compounds may prove to be distinct in their structures and properties because they can incorporate two different asymmetric building units, namely, $[Bi_xS_y]$ and $[As_xQ_y]$ in one structure. In addition, the introduction of bismuth to arsenic sulfide glasses has resulted in significantly enhanced conductivities.[7] To date, only three compounds have been reported in the literature: $Cs_4BiAs_3Se_7$, $(Me_4N)_2RbBiAs_6S_{12}$, and $K_3BiAs_3Se_6$.[8] We have employed the polychalcogenide flux method to the quaternary $Cs_2S/Bi/As/S$ system. An arsenic-poor flux gave rise to two new crystalline compounds containing $As^V$: $Cs_3Bi(AsS_4)_2$ containing one-dimensional (1D) chains of $[Bi(AsS_4)_2]^{3-}$ (referred to as **c1**) and $Cs_9Bi(AsS_4)_4$ containing discrete $[Bi(AsS_4)_4]^{9-}$ anions. With an arsenic-rich composition, we prepared four new chalcogenide glasses in the series $Cs_{n-1}BiAs_nS_{2n+1}$ where $n$ = 3, 4, 7, and 9, namely, $Cs_2BiAs_3S_7$ (**g1**), $Cs_4BiAs_4S_{11}$ (**g2**), $Cs_6BiAs_7S_{15}$ (**g3**), and $Cs_8BiAs_9S_{19}$ (**g4**). X-ray photoelectron spectroscopy (XPS) and Raman spectroscopic studies and pair distribution function (PDF) analysis suggest the presence of $As^{III}$-containing $As_nS_{2n+1}$ fragments in the glass structure. The fine-tuning of the polysulfide flux and its effect on the derived phases are discussed. The glasses (**g1**−**g4**) and **c1** show sharp absorption edges corresponding to the band gap in the range 1.51−2.3 eV. Thermal and optical behaviors of these compounds are correlated with their structures.

**Received:** June 28, 2013
**Published:** September 24, 2013

## EXPERIMENTAL SECTION

**Reagents.** The chemicals in this work were used as obtained: (i) sulfur powder, sublimed, 99.5%, 100 mesh, Alfa Aesar; (ii) cesium metals, analytical reagent, Johnson Matthey/AESAR Group, Seabrook, NH; (iii) bismuth, 99.999%, Noranda Advanced Materials, St. Laurent, Quebec, Canada; (iv) arsenic, 99.9%, Aldrich Chemical Co.; (v) *N*,*N*-dimethylformamide (DMF), ACS reagent grade, Spectrum Chemicals; (vi) diethyl ether, anhydrous, ACS reagent grade, Columbus Chemical Industries, Columbus, WI.

**Synthesis of $Cs_3Bi(AsS_4)_2$ (c1).** All manipulations were carried out under a dry nitrogen atmosphere in a Vacuum Atmospheres dry-lab glovebox. $Cs_2S$ was prepared by a modified literature procedure by reacting stoichiometric amounts of the elements in liquid ammonia.

A mixture of $Cs_2S$ (0.179 g, 0.60 mmol), bismuth (0.042 g, 0.20 mmol), arsenic (0.060 g, 0.80 mmol), and sulfur (0.115 g, 3.59 mmol) was loaded into a fused-silica tube in a nitrogen-filled glovebox. It was flame-sealed under vacuum ($\sim 10^{-4}$ mbar) and then heated to 500 °C in 5 h. After 60 h of soaking, it was cooled to 250 °C in 50 h, followed by rapid cooling to room temperature. The yellow compound was isolated as a single phase in >85% yield after dissolution of the excess flux with degassed DMF. Semiquantitative energy-dispersive spectroscopic (EDS) analysis gave an average composition of $Cs_{3.1}BiAs_{2.2}S_{8.4}$.[9]

**Synthesis of $Cs_9Bi(AsS_4)_4$ (c2).** A mixture of $Cs_2S$ (0.213 g, 0.72 mmol), bismuth (0.025 g, 0.12 mmol), arsenic (0.054 g, 0.72 mmol), and sulfur (0.054 g, 1.68 mmol) was loaded into a fused-silica tube in a nitrogen-filled glovebox and flame-sealed under vacuum ($\sim 10^{-4}$ mbar) and then heated to 500 °C in 5 h. After 60 h of soaking, it was cooled to 250 °C in 50 h, followed by rapid cooling to room temperature. A mixture of red (~92%), white (~5%), and yellow (~3%) compounds were isolated after removal of the excess flux with degassed DMF. Semiquantitative EDS analysis of several red crystals gave an average composition of $Cs_{9.1}BiAs_{4.2}S_{16.6}$.[10] The yellow crystals are identified as **c1**; however, the white crystals have not been identified as yet.

**Synthesis of $Cs_{n-1}BiAs_nS_{2n+1}$ ($n$ = 3, 5, 7, and 9) Glasses (g1−g4).** Four different chalcogenide glasses were synthesized by solid-state reactions of $Cs_2S$, bismuth, arsenic, and sulfur. In the original preparation, the respective stoichiometric mixtures were loaded into fused-silica tubes in a nitrogen-filled glovebox and flame-sealed under vacuum ($\sim 10^{-4}$ mbar) and then heated to 500 °C in 5 h. After 60 h of soaking at this temperature, they were cooled to 250 °C in 50 h, followed by rapid cooling to room temperature to form amorphous glassy materials. These glasses, however, can also be rapidly prepared by obtaining melts of the corresponding composition and solidifying them by quenching in air. The amorphous phases were confirmed by powder X-ray diffraction (PXRD). Below are the ratios used for the syntheses of glasses **g1**−**g4**.

$Cs_2BiAs_3S_7$ (**g1**): $Cs_2S$ (0.447 g, 1.50 mmol), Bi (0.314 g, 1.50 mmol), As (0.337 g, 4.51 mmol), and S (0.289 g, 9.02 mmol). $Cs_4BiAs_5S_{11}$ (**g2**): $Cs_2S$ (0.596 g, 2.0 mmol), Bi (0.209 g, 1.0 mmol), As (0.375 g, 5.0 mmol), and S (0.289 g, 9.0 mmol). $Cs_6BiAs_7S_{15}$ (**g3**): $Cs_2S$ (0.596 g, 2.0 mmol), Bi (0.139 g, 0.67 mmol), As (0.350 g, 4.66 mmol), and S (0.257 g, 7.98 mmol). $Cs_8BiAs_9S_{19}$ (**g4**): $Cs_2S$ (0.596 g, 2.0 mmol), Bi (0.105 g, 0.50 mmol), As (0.337 g, 4.51 mmol), and S (0.241 g, 7.54 mmol). The average compositions of the glassy phases are obtained by semiquantitative EDS analysis, and they agreed very well with the corresponding loading compositions.

## PHYSICAL MEASUREMENTS

**PXRD Analysis.** PXRD analyses were performed using a calibrated (against NIST silicon) CPS 120 INEL powder X-ray diffractometer (Cu K$\alpha$ graphite-monochromatized radiation) operating at 40 kV/20 mA and equipped with a position-sensitive detector with flat sample geometry. Theoretical PXRD patterns from single-crystal X-ray data were calculated using the *PowderCell*, version 2.3, software package.

**Electron Microscopy.** Semiquantitative microprobe analyses of the compounds were performed with a Hitachi S-3400 scanning electron microscope equipped with a PGT energy-dispersive X-ray analyzer. Data were acquired with an accelerating voltage of 25 kV and a 60 s accumulation time.

**Solid-State UV/vis/Near-IR Spectroscopy.** Optical diffuse-reflectance measurements were performed at room temperature using a Shimadzu UV-3101PC double-beam, double-monochromator spectrophotometer. The instrument is equipped with an integrating sphere detector and controlled by a computer. $BaSO_4$ was used as a 100% reflectance standard. The samples were prepared by grinding the crystals to a powder and spreading it on a compacted surface of the powdered standard material, preloaded into a sample holder. The reflectance versus wavelength data generated were used to estimate the band gap of the materials by converting reflectance to absorption data using the Kubelka−Munk equation as described in detail previously.[11]

**Raman Spectroscopy.** Raman spectra were recorded on a Biorad FT-Raman II spectrograph equipped with a Nd:YAG infrared continuous-wave laser ($\lambda$ = 1064 nm) and a liquid-nitrogen-cooled germanium detector. A finely powdered sample in a pyrex capillary tube was used for the spectral study after calibrating the spectrometer with KBr. The laser power at the sample was estimated to be about 5 mW, and the focused laser beam diameter was ca. 10 $\mu$m. A total of 20 scans were sufficient to obtain a good-quality spectrum.

**Differential Thermal Analysis (DTA).** Thermal analysis was performed on a Shimadzu DTA-50 thermal analyzer. Typically, a sample (~30 mg) of ground crystalline material was sealed in a silica ampule under vacuum. A similar ampule of equal mass filled with $Al_2O_3$ was sealed and placed on the reference side of the detector. The sample was heated to 600 °C at 10 °C/min and, after 1 min, was cooled at a rate of −10 °C/min to 50 °C. The residues of the DTA experiments were examined by PXRD. The reproducibility of the results was confirmed by running multiple heating/cooling cycles. The melting and crystallization points were measured at the minimum of the endothermic peak and at the maximum of the exothermic peak, respectively.

**Single-Crystal X-ray Crystallography for c1.** Data collections were done at 100 K using a STOE imaging-plate diffraction system (IPDS-2) with graphite-monochromatized Mo K$\alpha$ radiation. A numerical absorption correction was applied using the *X-area* suite programs. Face-indexed data were used to optimize the shape of the crystal using *X-Shape*. Direct methods and full-matrix least-squares refinement against $F^2$ were performed with the *SHELXTL* package. Initial indexing of all reflections gave a monoclinic unit cell. Systematic absences confirm the monoclinic space group $P2_1/c$. All atoms were found by running a few cycles of refinements. The crystallographic refinement details, fractional atomic coordinates, and anisotropic thermal parameters for **c1** are shown in Tables 1−3 (see the Supporting Information).

A full sphere of data was also collected at room-temperature (298 K) using a Bruker SMART CCD diffractometer employing Mo K$\alpha$ radiation. The structure was solved in the orthorhombic space group *Pnma*. Although the unit cell dimensions of the red crystals were close to those of $K_9Bi(PS_4)_4$[12] and EDS confirmed the stoichiometry of $Cs_9BiAs_4S_{16}$, we were unable to obtain a reasonable crystal structure refinement.

**PDF Analysis.** Powder samples of crystalline **c1** and three different glasses were packed in Kapton capillaries (1 mm diameter), and diffraction data were collected at 100 K using the rapid-acquisition PDF (RA-PDF) technique.[13] Data were


dx.doi.org/10.1021/ic4016542 | *Inorg. Chem.* 2013, 52, 11370−11376

collected using an MAR345 image-plate detector and 90.4 keV energy X-rays ($\lambda$ = 0.13702 Å) at the 6-IDD beamline at the Advanced Photon Source at Argonne National Laboratory. Measurements were done for 3 s and repeated around 150 times to improve counting statistics. The data were combined and integrated using the program *FIT2D*.[14] Various corrections were made to the data, such as subtraction of the background and container, Compton and fluorescence scattering, geometric corrections, absorption, etc.[15] Corrections were made using the program *PDFgetX2*.[16] Finally, $S(Q)$ was truncated at $Q_{max}$ of 20 Å$^{-1}$ before the PDF was calculated. Simulations were carried out using *PDFfit2*.[17]

**XPS.** XPS was acquired on an Omicron ESCA probe (Taunusstein, Germany) equipped with an Al K$\alpha$ X-ray source. Samples were analyzed at pressures between $10^{-9}$ and $10^{-8}$ Torr with a pass energy of 29.35 eV and a takeoff angle of 45°. All peaks were referenced to the signature C 1s peak for adventitious carbon at 284.6 eV to account for the charging effects. Powder glassy samples were mounted on copper tape on an aluminum sample holder and spread throughout the copper tape to minimize the charging effect. The areas of the peaks were computed after fitting the experimental spectra to Gaussian/Lorentzian curves and removing the background (Shirley function).

**Density Measurements.** The densities of the glassy materials were measured by a Micromeritics AccuPyc 1340 gas pycnometer (1 cm$^3$ model) using ultra-high-purity helium gas. About a 800 mg sample was taken for measurement. Analysis run cycles were continued until a standard deviation of ±0.0002 cm$^3$ was obtained for the sample volume.

## RESULTS AND DISCUSSION

**Synthesis.** The yellow crystalline compound **c1** was obtained by heating polysulfide flux mixtures of $Cs_2S$/Bi/As/S at 500 °C. A sulfur-rich mixture with ratio 1:1:1:8 led to **c1** along with a black impurity phase, which was confirmed to be $Bi_2S_3$. An attempt to synthesize phase-pure **c1** free of $Bi_2S_3$ by lowering the reaction temperature to 450 °C from 500 °C was unsuccessful. The $Cs_2S$/Bi/As/S polysulfide flux ratio of 2:0.5:2:8 led to ~90:10 mixtures of yellow (**c1**) and red (possibly **c2**) crystalline compounds. We obtained phase-pure **c1** when the $Cs_2S$ fraction in the $Cs_2S$/Bi/As/S polysulfide flux was decreased to 1.5:0.5:2:9 as determined by PXRD (Figure 1a).

Increasing the amount of $Cs_2S$ (3:1:1:8) resulted in a new red crystalline compound along with **c1** and $Bi_2S_3$. Elemental analysis confirmed the stoichiometry of the red compound to be **c2**, and the unit cell dimensions were similar to those of $K_9Bi(PS_4)_4$.[12] A much higher yield of **c2** (~90%) was obtained from a polysulfide flux ratio of 3:0.5:3:7. The significant role of the flux basicity ($Cs_2S$/S ratio) on the reaction outcome is certainly highlighted in the above results.

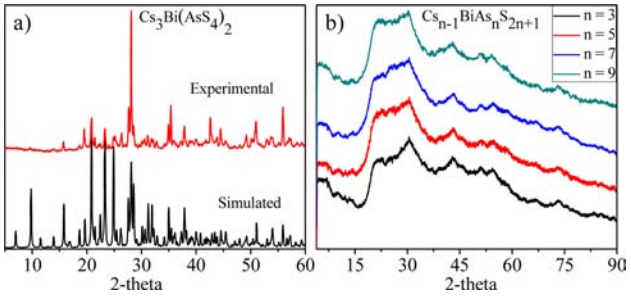


**Figure 1.** (a) Comparison of the PXRD patterns: simulated pattern from the single-crystal X-ray structure with that of bulk compound **c1**. (b) PXRD patterns of four different glasses in the series $Cs_{n-1}BiAs_nS_{2n+1}$: $Cs_2BiAs_3S_7$ ($n$ = 3), $Cs_4BiAs_5S_{11}$ ($n$ = 5), $Cs_6BiAs_7S_{15}$ ($n$ = 7), and $Cs_8BiAs_9S_{19}$ ($n$ = 9).

Because the above reactions gave crystalline compounds of the $[AsS_4]^{3-}$ $As^V$ species, we increased the arsenic fraction in the reaction mixtures of $Cs_2S$/Bi/As/S, in an attempt to stabilize compounds with the $As^{III}$ species. These reactions, however, led to the formation of dark-red glassy compounds. The PXRD pattern of the dark-red samples confirms their amorphous nature (Figure 1b). Four new glassy compounds in the series $Cs_{n-1}BiAs_nS_{2n+1}$ were obtained by melt-quenching the corresponding direct mixtures of $Cs_2S$/Bi/As/S. EDS analysis by scanning electron microscopy (SEM) confirms the presence of all four elements in the glass (Figure 2a). A sample ingot of **g1** glass was cut and polished, and SEM elemental surface mapping was performed to check the distribution of individual elements in the glass (Figure 2b). A fairly homogeneous distribution of individual elements within the glass matrix is evident from the positions of the green spots (Figure 2b).

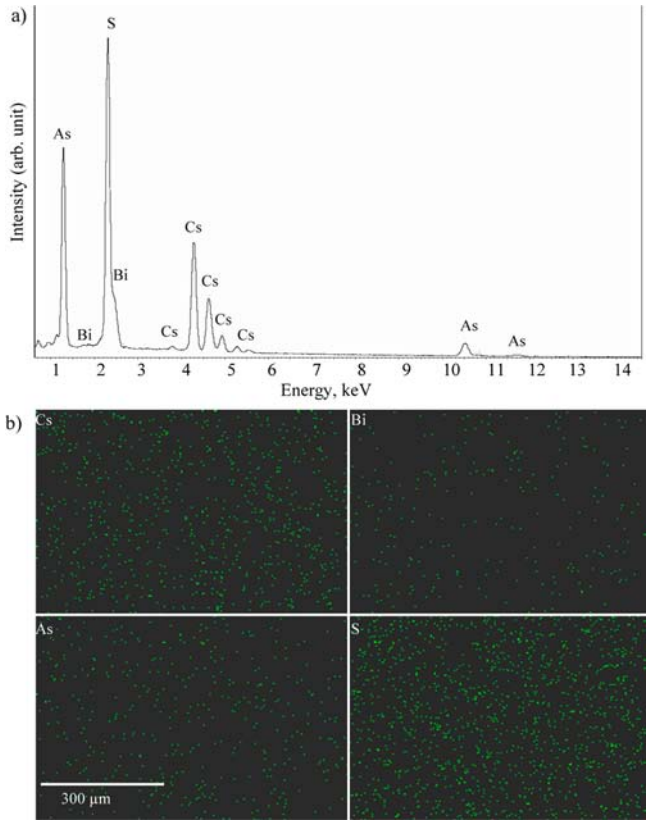


**Figure 2.** (a) EDS spectrum of the **g1** glass showing the presence of all four elements. (b) SEM elemental mapping for individual elements of the **g1** glass sample shows a fairly homogeneous distribution of elements within the glass.

The mass densities of the glassy samples were measured using helium pycnometry. Helium, which can enter even the smallest voids or pores, was used to measure the unknown volume in the glass with a known weight. The final result is referred to as the skeletal density. The skeletal densities of **g1**–**g4** glasses are 4.02, 3.76, 3.66, and 3.60 g/cm$^3$, respectively.


dx.doi.org/10.1021/ic4016542 | *Inorg. Chem.* 2013, 52, 11370–11376

There is a gradual decease of the density with increasing $n$ in the $Cs_{n-1}BiAs_nS_{2n+1}$ glass series, which reflects the smooth compositional changes occurring with increasing $n$.

**Crystal Structure of c1.** The structure of **c1** features 1D chains of $^1/_\infty[Bi(AsS_4)_2]^{3-}$ running down the $b$ axis (Figure 3a). The chains are made up of five-coordinate Bi atoms

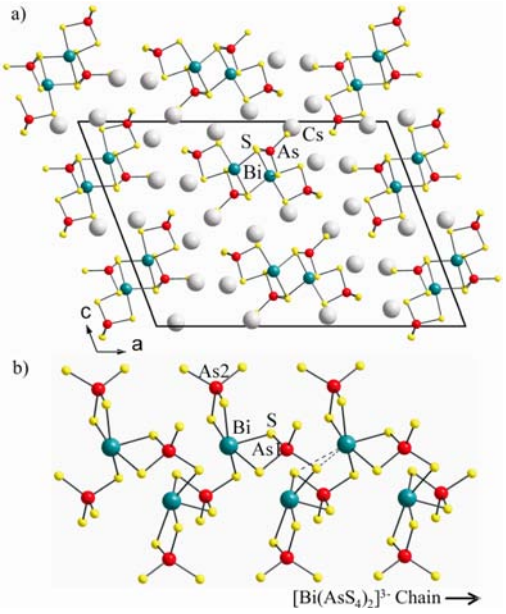


**Figure 3.** (a) Unit cell view of **c1** down the $b$ axis showing the packing of $^1/_\infty[Bi(AsS_4)_2]^{3-}$ chains. (b) View of the $^1/_\infty[Bi(AsS_4)_2]^{3-}$ chains. The zigzag arrangement of the Bi atoms along the chain direction is evident from the picture.

arranged in a zigzag fashion (Figure 3b). Each Bi atom is coordinated by three tetrahedral $[AsS_4]^{3-}$ anions, two of which coordinate using an edge and one in a corner-sharing fashion. As mentioned earlier, our investigation in this system was also an attempt to introduce asymmetric $[Bi_mS_n]$ units in the structure. The structure clearly shows this asymmetric $[BiS_5]$ square pyramid along with the stereochemical expression of the Bi $6s^2$ lone pair (Figure 3b). There are two different kinds of $[AsS_4]^{3-}$ ligands. The $[As(1)S_4]^{3-}$ tetrahedron coordinates to two Bi atoms by using an edge and corners that serve to propagate the chain. The $[As(2)S_4]^{3-}$ tetrahedron is a terminal ligand and uses an edge to bind to the Bi atoms (chelate; Figure 3b). The Bi–S distances range from 2.630(6) to 2.965(4) Å, and two long Bi–S interactions at distances of 3.446(2) and 3.513(2) Å are shown by the dotted line in Figure 3b. The As–S distances are similar to those of previously reported $[AsS_4]^{3-}$-containing compounds and range from 2.100(4) to 2.262(6) Å.[18] The Cs atoms surround the chains, and an electrostatic interaction between $Cs^+$ ions and $^1/_\infty[Bi(AsS_4)_2]^{3-}$ chains holds the structure together.

The structure of **c1** is similar to that of $Cs_3Bi(PS_4)_2$ except that the latter crystallizes in the noncentrosymmetric space group $P2_12_12_1$ and does not exhibit Bi disorder.[19] These chains are also related to $K_3La(PS_4)_2$[20] and $K_3La(PSe_4)_2$,[21] except that the La is nine-coordinated by four $PS_4^{3-}$ units in edge- and face-sharing modes.

We observed that **c1** undergoes a phase transition from monoclinic at 100 K to orthorhombic at 300 K. The structural description of the orthorhombic structure is essentially the same as that of the monoclinic one except that there is only one disordered crystallographic Bi site.

**X-ray Photoelectron Spectroscopy (XPS).** In order to elucidate the oxidation state of arsenic in the $Cs_2S/Bi/As/S$ glasses, XPS spectra of the **g1** glass were compared with those of the $As^{III}$-containing $As_2S_3$[22] and $As^V$-containing crystalline compound $Cs_3BiAs_2S_8$ (**c1**). The glassy sample of **g1** showed As 4d peaks with binding energies of 42.6 eV ($4d_{3/2}$) and 43.5 eV ($4d_{1/2}$), which are close to those of $As_2S_3$ (42.2 and 43.3 eV) and comparable to those of other $As^{III}$-containing materials (Figure 4).[23]

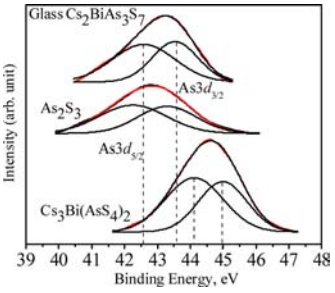


**Figure 4.** As 4d binding energy peaks in the XPS spectrum of the **g1** glass compared with that of $As_2S_3$ and the crystalline compound **c1**.

The similarity of the As 4d binding energies for **g1** and $As_2S_3$ suggests the presence of $As^{III}$ species in the glass. The spectrum also lacks features that might be attributed to any adventitious $As^{IV}$ species. By contrast, the higher As 4d binding energy peaks of 44.1 and 45 eV for the $As^V$-containing crystalline material **c1** is in accordance with the presence of the tetrahedral $[AsS_4]^{3-}$ anion.

**Structural Fragments in $Cs_{n-1}BiAs_nS_{2n+1}$ Glasses.** The presence of $[As_3S_7]^{5-}$ fragments in the **g1** glass was assumed from the knowledge of the previously reported $[As_3S_7]^{5-}$-containing compound $(Ph_4P)_2InAs_3S_7$.[8b] The $[As_3S_7]^{5-}$ fragment in $(Ph_4P)_2InAs_3S_7$ is constructed from the corner sharing of three $AsS_3$ pyramids (Figure 5a). Larger $[As_nS_{2n+1}]$ fragments with more $AsS_3$ units are also possible, e.g., $[As_5S_{11}]^{7-}$, $[As_7S_{15}]^{9-}$, and $[As_9S_{19}]^{11-}$ (Figure 5).[24] Therefore, a series of glasses with the formula $Cs_{n-1}BiAs_nS_{2n+1}$ (where $n$ = 1, 2, 3, etc.), likely with 1D structures, can be realized.

The presence of cesium is necessary for stabilization of the glass because the composition "$BiAsS_3$" (when $n$ = 1) does not form a stable glass or a crystalline compound and instead comprises a mixture of crystalline $Bi_2S_3$ and glassy $As_2S_3$. A recent study by Voynarovych et al. also failed to stabilize $Bi_2S_3/As_2S_3$ glasses.[25] In the present study, stable glasses of $Cs_{n-1}BiAs_nS_{2n+1}$ were obtained with $n \geq 3$. Therefore, the glass formation tendency is greater with comparatively large $[As_nS_{2n+1}]$ fragments than with the smaller ones such as $[AsS_3]^{3-}$ or $[As_2S_5]^{4-}$.

**Raman Spectroscopy.** A comparative Raman spectroscopic study of the glasses **g1**–**g4** and crystalline **c1** was conducted to elucidate the types of structural fragments in the chalcogenide glass. As expected, **c1** showed sharp peaks in the Raman spectrum compared to those of the glasses (Figure 6). The high energy peaks in the range of 310–470 $cm^{-1}$ are assigned to the As–S stretching modes, the peak at 280 $cm^{-1}$ can be assigned to Bi–S stretching vibration, and the weak bands situated at ~191 $cm^{-1}$ can be attributed to the bending modes of $AsS_3$ pyramids.[26] The As–S stretching peaks in the


dx.doi.org/10.1021/ic4016542 | Inorg. Chem. 2013, 52, 11370–11376

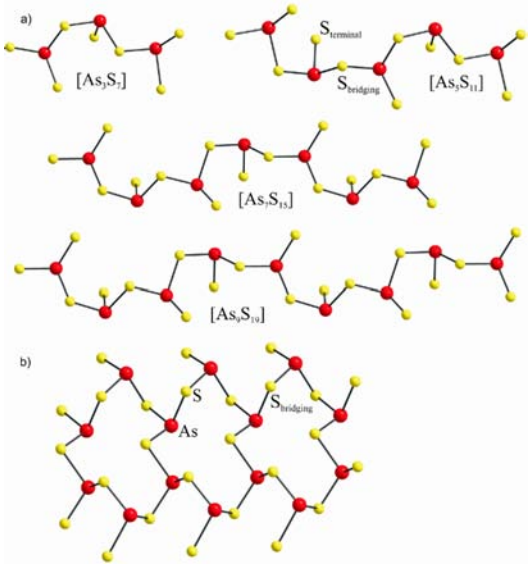


**Figure 5.** (a) Four different $[As_nS_{2n+1}]$ fragments generated by varying the number of As atoms from 3 to 9. The presence of both bridging S and terminal S atoms can be clearly seen. (b) View of the layer in $As_2S_3$ showing the presence of only bridging S atoms. These were reproduced from the published ref 8b, 22, and 24.

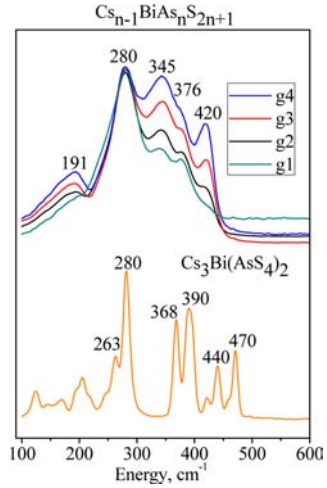


**Figure 6.** Raman spectra of $Cs_{n-1}BiAs_nS_{2n+1}$ glasses **g1**–**g4** and crystalline **c1**.

$Cs_{n-1}BiAs_nS_{2n+1}$ glasses are shifted to lower frequencies compared to the peaks of **c1** because of the longer $As^{III}$–S bonds relative to the $As^{V}$–S bonds.[6a] This is also supported by the PDF analysis results presented below.

The Raman spectra of all four glasses (**g1**–**g4**) are closely related, which suggests the presence of similar structural fragments. The intensity of the As–S stretching peaks for the $Cs_{n-1}BiAs_nS_{2n+1}$ series increases gradually with increasing $n$ (i.e., on going from **g1** to **g4**), while the intensity of the Bi–S stretching peak remains similar between the four glasses (Figure 6). This is consistent with the relative content of arsenic and bismuth in **g1**–**g4** glasses. The wide spreading of As–S stretching bands in the spectral region between 345 and 420 $cm^{-1}$ can be accounted for by the increased distribution of the As–S distances and S–As–S angles in the glasses compared to crystalline $As_2S_3$. The latter exhibits As–S stretching peaks in a comparatively narrower range of 343–373 $cm^{-1}$.[26] The increased distribution of the As–S distances within the glass (in comparison to $As_2S_3$) can result from both the fragmentation of the two-dimensionally layered structure of $As_2S_3$ (see Figure 5b) into $[As_nS_{2n+1}]$ segments and the induced strain from the randomness of the structure (Figure 5a).[27] A similar spreading of As–S stretching bands was seen in the Raman spectra of $LiAsS_2$ and $NaAsS_2$, which have 1D As–S chains built of corner-sharing $AsS_3$ pyramids.[2d]

Each $AsS_3$ unit within the $[As_nS_{2n+1}]$ fragment in Figure 5a has two different S atoms: terminal $\mu_1$- and bridging $\mu_2$-S atoms. The terminal S atom has the tendency to form strong S 4p to As 4p back-$\pi$-bonding, resulting in shorter As–S bond distances (~2.17 Å) compared to the bridging As–S distances (~2.32 Å), as observed in $LiAsS_2$ and $NaAsS_2$.[2d] $As_2S_3$, on the other hand, has only bridging S atoms, resulting in very similar As–S bond distances (Figure 5b). Therefore, the high-energy peak at 420 $cm^{-1}$ in the Raman spectra of the glasses can be assigned to the $As–S_{terminal}$ stretching mode, and the medium-energy peaks at 345 and 376 $cm^{-1}$ can be assigned to the $As–S_{bridging}$ stretching modes. There is no signature of the S–S bonds in the glass, which is generally indicated by a peak at 480–495 $cm^{-1}$.

**Local Structure with PDF Analysis.** PDF analysis of crystalline **c1** was compared with that of the $Cs_{n-1}BiAs_nS_{2n+1}$ glasses **g1**, **g2**, and **g4** to determine the local coordination of the constituent atoms. The PDF of the glasses show well-defined peaks up to ~8 Å. Above ~8 Å, the interatomic correlations in the glass disappear, indicating the lack of long-range periodicity (Figure 7a). On the basis of the relative

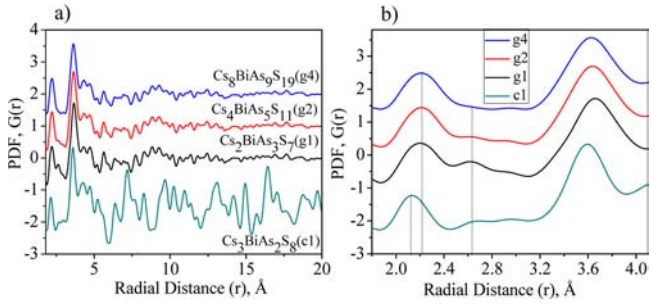


**Figure 7.** PDF of crystalline **c1** compared with that of the $Cs_{n-1}BiAs_nS_{2n+1}$ glasses **g1**, **g2**, and **g4**: (a) $r$ = 1.8–20 Å; (b) $r$ = 1.8–4.1 Å.

atom–atom distances in **c1**, the strong peak at ~2.15 Å is attributed to the As–S bonds, the weak peaks at ~2.75 Å are associated with the Bi–S bonds, and the strong peak at ~3.60 Å is correlated to the Cs–S bonds in the structure (Figure 7b). An upshifting of the As–S correlation for the glasses relative to **c1** indicates longer As–S bond distances in the glasses (Figure 7b). This is in accordance with the XPS and Raman spectroscopic studies discussed above, and it is consistent with the presence of $As^{III}$ species in the glasses.

**UV/Vis/Near-IR Electronic Absorption Spectroscopy.** The optical absorption properties of glassy **g1**–**g4** and crystalline **c1** were investigated with UV/vis/near-IR diffuse-reflectance spectroscopy. The glassy materials show sharp absorption edges corresponding to energy band gaps of 1.51, 1.76, 1.68, and 1.81 eV for **g1**–**g4**, respectively (Figure 8a). The gradual increase of the band-gap size on going from **g1** to **g4** is consistent with a decreasing Bi/As fraction, which affects band-edge formation.[28] Figure 8b shows the optical absorption


dx.doi.org/10.1021/ic4016542 | Inorg. Chem. 2013, 52, 11370–11376

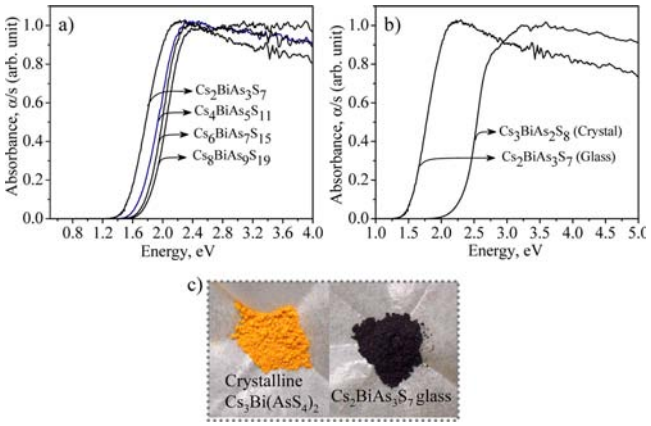


**Figure 8.** (a) Solid-state UV/vis optical absorption spectra of the $Cs_{n-1}BiAs_nS_{2n+1}$ glasses **g1**–**g4**. (b) Comparison of the UV/vis optical absorption edges between the crystalline **c1**, $E_g$ = 2.32 eV and **g1**, $E_g$ = 1.51 eV. (c) Powder samples of **c1** and **g1**.

edge at 2.33 eV for **c1**. The smaller band gap of the **g1** glass compared to the crystalline compound **c1** can be visually seen in Figure 8c. Although glassification of a crystalline compound typically results in only a few tenths of an electronvolt decrease in the band-gap size, as is seen in the case of the recently reported chalcophosphates $APSe_6$ and $A_2P_2Se_6$ (A = K, Rb, Cs);[29] the origin of such a high difference in the present case is difficult to assess because of the different compositions of the two types of compounds. The observed 0.81 eV decrease in the band gap of **g1** compared to **c1** may be due to the higher Cs content (and lower dimensionality of the Bi/As/S framework in the compound) in **c1**.

**Thermal Behavior.** DTA of the crystalline and glassy compounds shows a single endothermic melting peak at 407 °C and two exothermic peaks at 310 and 380 °C, one of which can be ascribed to crystallization of **c1** (Figure 9a). The second exothermic peak in the DTA plot of **c1** can be assigned to crystallization of the decomposition product (Figure 9a). PXRD of the sample after DTA indicated the presence of $Bi_2S_3$. The solid-state UV/vis optical absorption study also confirms the presence of $Bi_2S_3$ in the recovered compound after DTA (Figure 9b). The polysulfide flux is therefore critical for isolation of **c1** in pure single-crystalline form.

Although the powder glassy sample of **g1** became a fused large ingot after DTA, we did not observe thermal characteristics corresponding to crystallization, melting, or glass transitions. This may be because of the small energy difference between the molten and glassy phases of **g1**. Such transitions generally appear as exothermic (crystallization) and endothermic (melting) events, respectively.[29a] Nevertheless, PXRD of the sample after DTA showed the presence of $Bi_2S_3$, suggesting thermal decomposition upon heating (Figure 9c). Hence, it can be concluded that the quaternary Cs/Bi/As/S phases are only kinetically stable.

## ■ CONCLUDING REMARKS

The synthesis of the new crystalline $[As^VS_4]^{3-}$-containing compounds, **c1** and **c2**, was achieved by the proper tuning of the basicity of a low arsenic-containing $Cs_2S/Bi/As/S$ flux. The structures feature tetrahedral $[As^VS_4]^{3-}$ connected to $Bi^{3+}$ centers to give infinite $^1/_\infty[Bi(AsS_4)_2^{3-}]$ chains and discrete molecular complexes of $[Bi(AsS_4)_4]^{9-}$. On the other hand, the use of an arsenic-rich flux stabilizes the more reduced $As^{III}$ species and favors glass formation. In this manner, four different sulfide glasses of the formula $Cs_{n-1}BiAs_nS_{2n+1}$ were synthesized. Thus, controlling the arsenic fraction could be a useful synthetic approach to preparing broad varieties of chalcoarsenate building blocks and novel chalcogenide glasses. To assess the processability, it would be interesting to attempt glass fiber

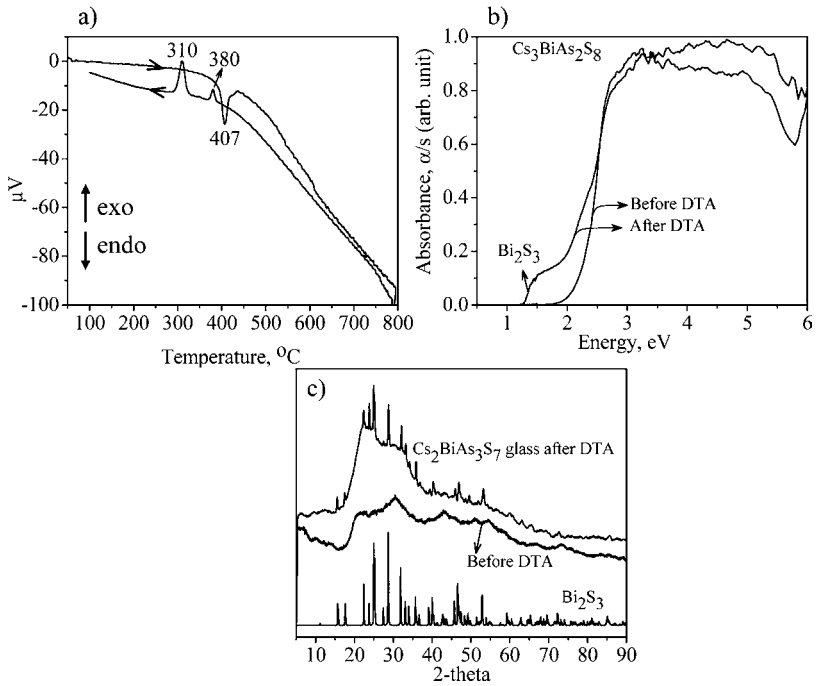


**Figure 9.** (a) DTA plot of **c1** showing a single exothermic peak upon heating and two endothermic peaks upon cooling. (b) Solid-state UV/vis optical absorption spectra of **c1** before DTA and after DTA. (c) Overlay of the PXRD pattern of $Bi_2S_3$, **g1** glass before DTA, and **g1** after DTA. Thermal decomposition of **g1** is clearly evident from the appearance of sharp diffraction peaks corresponding to $Bi_2S_3$.


dx.doi.org/10.1021/ic4016542 | Inorg. Chem. 2013, 52, 11370–11376

drawing from the melts of the series for further optical infrared investigations.

## ■ ASSOCIATED CONTENT

### Supporting Information

X-ray crystallographic files (CIF), crystallographic refinement details, atomic coordinates with equivalent isotropic displacement parameters, anisotropic displacement parameters, and selected bond distances for **c1**. This material is available free of charge via the Internet at http://pubs.acs.org.

## ■ AUTHOR INFORMATION


### Corresponding Author

*E-mail: m-kanatzidis@northwestern.edu.


### Notes

The authors declare no competing financial interest.

## ■ ACKNOWLEDGMENTS

Financial support from the National Science Foundation (Grant DMR-1104965) is gratefully acknowledged. This work made use of the SEM facilities at the Electron Probe Instrumentation Center, Northwestern University. The FT-Raman spectroscopic study was done at the Analytical Service Laboratory, Northwestern University. Use of the Advanced Photon Source at Argonne National Laboratory was supported by the U.S. Department of Energy, Office of Science, Office of Basic Energy Sciences, under Contract No. DE4-AC02406CH11357.

## ■ REFERENCES


(1) (a) Kanatzidis, M. G.; Sutorik, A. C. *Prog. Inorg. Chem.* **1995**, *43*, 151. (b) Sunshine, S. A.; Kang, D.; Ibers, J. A. *J. Am. Chem. Soc.* **1987**, *109*, 6202. (c) Bera, T. K.; Iyer, R. G.; Malliakas, C. D.; Kanatzidis, M. G. *Inorg. Chem.* **2007**, *44*, 8466. (d) Iyer, R. G.; Kanatzidis, M. G. *Inorg. Chem.* **2004**, *43*, 3656.

(2) (a) Ye, N.; Chen, Q.; Wu, B.; Chen, C. *J. Appl. Phys.* **1998**, *84* (1), 555−558. (b) Distanov, V. E. ; Nenashev, B. G.; Kirdyashkin, A. G.; Serboulenko, M. G. *J. Cryst. Growth* **2002**, *235*, 457. (c) Feichtner, J. D.; Roland, G. W. *Appl. Opt.* **1972**, *11*, 993. (d) Bera, T. K.; Song, J. H.; Freeman, A. J.; Jang, J. I.; Ketterson, J. B.; Kanatzidis, M. G. *Angew. Chem., Int. Ed.* **2008**, *47*, 7828. (e) Bera, T. K.; Jang, J. I.; Ketterson, J. B.; Kanatzidis, M. G. *J. Am. Chem. Soc.* **2009**, *131*, 75. (f) Song, J. H.; Freeman, A. J.; Bera, T. K.; Chung, I.; Kanatzidis, M. G. *Phys. Rev. B* **2009**, *79*, 245203. (g) Bera, T. K.; Song, J. H.; Freeman, A. J.; Jang, J. I.; Ketterson, J. B.; Kanatzidis, M. G. *J. Am. Chem. Soc.* **2010**, *132*, 3484.

(3) (a) Phillips, J. C. *J. Non-Cryst. Solids* **1979**, *34*, 151. (b) Bureau, B.; Boussard-Pledel, C.; Lucas, P.; Zhang, X.; Lucas, J. *Molecules* **2009**, *14*, 4337.

(4) (a) Liang, Z. *J. Non-Cryst. Solids* **1991**, *127*, 298. (b) Shiryaev, V. S.; Churbanov, M. S. *J. Non Cryst. Solid* **2013**, http://dx.doi.org/10.1016/j.jnoncrysol.2012.12.048. (c) Houizot, P.; Boussard-Plédel, C.; Faber, A. J.; Cheng, L. K.; Bureau, B.; Van Nijnatten, P. A.; Gielesen, W. L. M.; Pereira do Carmo, J.; Lucas, J. *Opt. Express* **2007**, *15*, 12529.

(5) (a) Eggleton, B. J.; Luther-Davies, B.; Richardson, K. *Nat. Photonics* **2011**, *5*, 141. (b) El-Amraoui, M.; Smektala, F. *Opt. Express* **2010**, *18*, 26655. (c) Hughes, M. A.; Akada, T.; Suzuki, T.; Ohishi, Y.; Hewak, D. W. *Opt. Express* **2009**, *17*, 19345.

(6) (a) Shoemaker, D. P.; Chung, D. Y.; Mitchell, J. F.; Bray, T. H.; Soderholm, L.; Chupas, P. J.; Kanatzidis, M. G. *J. Am. Chem. Soc.* **2012**, *134*, 9456−9463. (b) Bera, T. K.; Kanatzidis, M. G. *Inorg. Chem.* **2008**, *47*, 7068. (c) Bera, T. K.; Kanatzidis, M. G. *Inorg. Chem.* **2012**, *51*, 4293.

(7) Siljegovic, M. V.; Lukic, S. R.; Skuban, F.; Petrovic, D. M.; Slankamenac, M. *J. Optoelectron. Adv. Mater.* **2009**, *11*, 204.

(8) (a) Wachhold, M.; Kanatzidis, M. G. *Z. Anorg. Allg. Chem.* **2000**, *626*, 1901. (b) Chou, J.-H.; Kanatzidis, M. G. *Inorg. Chem.* **1994**, *33*, 1001. (c) Wu, Y.; Bensch, W. *J. Alloys Compd.* **2011**, *509*, 4452.

(9) We also synthesized the related $Rb_3BiAs_2S_8$ from a mixture of $Rb_2S/Bi/As_2S_3/S$ in the ratio 1.5:1:1:3.5 at 500 °C using the same heating profile as that used for $Cs_3BiAs_2S_8$. The product was obtained as yellow plates in approximately 10% yield. EDS gave an average composition of $Rb_{3.4}BiAs_{2.2}S_{8.3}$. This compound crystallizes in the orthorhombic space group *Pnma*. Crystallographic details are provided in the Supporting Information.

(10) We also prepared the potassium and rubidium analogues of $Cs_9BiAs_4S_{16}$. $K_9BiAs_4S_{16}$ was prepared as red cubes from a 1.5:1:1:3.5 mixture of $K_2S/Bi/As_2S_3/S$, while $Rb_9BiAs_4S_{16}$ was synthesized as red plates from a 2:1:1:10 mixture of $Rb_2S/Bi/As/S$ at 500 °C. Both compounds crystallize in the orthorhombic space group $P2_12_12$ (data collected at 293 K). Crystallographic details can be found in the Supporting Information.

(11) (a) Johnsen, S.; Peter, S. C.; Nguyen, S. L.; Song, J. H.; Jin, H.; Freeman, A. J.; Kanatzidis, M. G. *Chem. Mater.* **2011**, *23*, 4375. (b) Liao, J. H.; Kanatzidis, M. G. *Chem. Mater.* **1993**, *5*, 1561.

(12) Gave, M. A.; Weliky, D. P.; Kanatzidis, M. G. *Inorg. Chem.* **2007**, *46*, 11063.

(13) Chupas, P. J.; Qiu, X. Y.; Hanson, J. C.; Lee, P. L.; Grey, C. P.; Billinge, S. J. L. *J. Appl. Crystallogr.* **2003**, *36*, 1342.

(14) Hammersley, A. P.; Svensson, S. O.; Hanfland, M.; Fitch, A. N.; Hausermann, D. *High Pressure Res.* **1996**, *14*, 235.

(15) Egami, T.; Billinge, S. J. L. *Underneath the Bragg Peaks: Structural Analysis of Complex Materials*; Pergamon Press: Amsterdam, The Netherlands, 2003.

(16) Qiu, X.; Thompson, J. W.; Billinge, S. J. L. *J. Appl. Crystallogr.* **2004**, *37*, 678.

(17) Farrow, C. L.; Juhas, P.; Liu, J. W.; Bryndin, D.; Bozin, E. S.; Bloch, J.; Proffen, T.; Billinge, S. J. L. *J. Phys.: Condens. Matter* **2007**, *19*, 335219.

(18) (a) Wu, Y.; Naether, C.; Bensch, W. *Inorg. Chem.* **2006**, *45*, 8835. (b) Schimek, G. L.; Kolis, J. W. *Acta Crystallogr., Sect. C* **1997**, *C53*, 991. (c) Iyer, R. G.; Kanatzidis, M. G. *Inorg. Chem.* **2004**, *43*, 3656. (d) Iyer, R. G.; Do, J.; Kanatzidis, M. G. *Inorg. Chem.* **2003**, *42*, 1475.

(19) McCarthy, T.; Kanatzidis, M. G. *J. Alloys Compd.* **1996**, *236*, 70.

(20) Evenson, C. R.; Dorhout, P. K. *Inorg. Chem.* **2001**, *40*, 2884.

(21) Evenson, C. R.; Dorhout, P. K. *Inorg. Chem.* **2001**, *40*, 2875.

(22) Mullen, D. J. E.; Nowacki, W. *Z. Kristallogr.* **1972**, *136*, 48.

(23) Li, W. Y.; Seal, S.; Rivero, C.; Lopez, C.; Richardson, K.; Pope, A.; Schulte, A.; Myneni, S.; Jain, H.; Antoine, K.; Miller, A. C. *J. Appl. Phys.* **2005**, *98*, 053503.

(24) (a) Sheldrick, W. S.; Wachhold, M. *Coord. Chem. Rev.* **1998**, *176*, 211. (b) Drake, G. W.; Kolis, J. W. *Coord. Chem. Rev.* **1994**, *137*, 131. (c) Dehnen, S.; Melullis, M. *Coord. Chem. Rev.* **2007**, *251*, 1259.

(25) Voynarovych, I.; Pinzenik, V.; Makauz, I.; Shiplyak, M.; Kokenyesi, S.; Daroczi, L. *J. Non-Cryst. Solids* **2007**, *353*, 1478.

(26) (a) Iovu, M. S.; Shutov, S. D.; Andriesh, A. M.; Kamitsos, E. I.; Varsamis, C. P. E.; Furniss, D.; Seddon, A. B.; Popescu, M. *J. Non-Cryst. Solids* **2003**, *326*, 306. (b) Kamitsos, E. I.; Kapoutsis, J. A.; Culeac, I. P.; Iovu, M. S. *J. Phys. Chem. B* **1997**, *101*, 11061.

(27) Minceva-Sukarova, B.; Jovanovski, G.; Makreski, P.; Soptrajanov, B.; Griffith, W.; Willis, R.; Grzetic, I. *J. Mol. Struct.* **2003**, *651*, 181.

(28) (a) Yao, J. Y.; Deng, B.; Ellis, D. E.; Ibers, J. A. *Inorg. Chem.* **2002**, *41*, 7094. (b) Chung, I.; Song, J. H.; Jang, J. I.; Freeman, A. J.; Ketterson, J. B.; Kanatzidis, M. G. *J. Am. Chem. Soc.* **2009**, *131*, 2647.

(29) (a) Chung, I.; Malliakas, C. D.; Jang, J. I.; Canlas, C. G.; Weliky, D. P.; Kanatzidis, M. G. *J. Am. Chem. Soc.* **2007**, *129*, 14996. (b) Chung, I.; Do, J.; Canlas, C. G.; Weliky, D. P.; Kanatzidis, M. G. *Inorg. Chem.* **2004**, *43*, 2762.